

This is a peer-reviewed, accepted author manuscript of the following research article: Hu, Y, Cheng, Y, Dai, S, Yuan, Z & Incecik, A 2026, 'Hydroelastic performance of a flexible pontoon-type floating breakwater embedded with multiple oscillating-water-column devices', *Renewable Energy*, vol. 259, 125065. <https://doi.org/10.1016/j.renene.2025.125065>

Hydroelastic performance of a flexible pontoon-type floating breakwater embedded with multiple oscillating-water-column devices

Yinong Hu^a, Yong Cheng^{a,*}, Saishuai Dai^b, Zhiming Yuan^{a,b}, Atilla Incecik^b

^a*School of naval architecture and ocean engineering, Jiangsu University of Science and Technology, Zhenjiang, 212003, China*

^b*Naval Architecture, Ocean and Marine Engineering Department, University of Strathclyde, Glasgow, United Kingdom*

Abstract

Combining Wave Energy Converters (WECs) with a long-flexible floating breakwater is a plausible pathway to the engineering application of wave energy technologies, which not only enhances energy capture capability but also improves structural stability of breakwater. This study proposes a multi-module flexible pontoon-type floating breakwater integrated with oscillating water column (OWC) units. Each chamber features an independent power take-off (PTO) system for energy capture. A coupled fluid-structure interaction model, integrating Computational Fluid Dynamics (CFD) with Finite Element Method (FEM), is developed to investigate the hydroelastic response. The bi-directional coupled process is realized by satisfying constant boundary conditions between fluid velocity and pressure, and structural node displacements at each time step. Parametric studies demonstrate that flexible structures offer superior adaptability to wave loading compared to rigid counterparts, effectively reducing wave-induced forces while maintaining energy capture. Further analysis reveal that increased structural stiffness enhances internal resonance within chambers, significantly improving capture factors, whereas excessive flexibility can trigger complex multimode radiated wave interactions, adversely affecting energy conversion efficiency. Additionally, incorporating a bottom opening strengthens wave resonance within the chamber, thereby increasing energy dissipation. These findings highlight practical advantages of multi-module flexible floating breakwaters, providing valuable guidelines for design and optimization in engineering applications.

Keywords: Array Oscillating Water Columns; Flexible Floating Breakwater; Fluid-Structure Interaction; Wave energy conversion; Hydroelastic response; Separate power take-off unit

*Corresponding author: Yong Cheng, mainly research in hydrodynamic performance of marine energy systems
E-mail: chengyong@just.edu.cn

List of abbreviations:

Nomenclature		
<i>Symbols</i>	<i>Abbreviations</i>	
L_b	Breakwater length [m]	
B_d	Breakwater width [m]	
b	Chamber width [m]	
a	Orifice opening [-]	
c	Bottom opening of chamber [m]	
d_b	Breakwater draft [m]	
h_b	Breakwater freeboard height [m]	
l_0	Chamber spacing [m]	
h	Water depth [m]	
λ	Wavelength [m]	
ζ	Capture factor [Nm ²]	
EI	Bending stiffness	
K_r	Reflection coefficient [-]	
K_t	Transmission coefficient [-]	
	OWC	Oscillating Water Column
	CFD	Computation Fluid Dynamics
	FEM	Finite Element Methods
	PTO	Power Take-Off
	FSI	Fluid Structure Interaction
	WEC	Wave Energy Converter
	OB	Oscillating Buoy
	NWT	Numerical Wave Tank
	RANS	Reynolds-Averaged Navier-Stokes
	VOF	Volume of Fluid
	WG	Wave Gauge

1. Introduction

As offshore operations increasingly contribute to the global economy, the importance of protecting coastal ports, harbors, and offshore facilities has become more prominent. Due to factors such as seabed-induced wave breaking, shoaling, wave refraction and higher-order interactions during wave propagation, coastal structures like docks and sea walls often face intense wave loads. As a piece of coastal infrastructure, breakwaters effectively dissipate wave energy from open seas and play a key role in withstanding wave impacts and protecting coastal areas. Compared to fixed breakwaters, floating breakwaters offer more advantages, the most significant of which is their applicability in deep water. They are less affected by geological conditions, have lower construction costs, and cause less environmental impact.

Wave energy is currently considered one of the most promising marine renewable energy resources, attracting numerous researchers due to its high availability, predictability, and high energy density[1]. Despite these advantages, one of the bottlenecks limiting the further development of wave energy devices is their high construction cost, primarily due to complex infrastructure and low capture factor. An effective way to reduce construction costs is to integrate wave energy devices into other marine engineering structures, thereby enabling the sharing of infrastructure[2].

Compared to traditional breakwaters, researchers are more inclined to study new types of floating breakwater-wave energy integrated devices. Michailides and Angelides[3] used a linear hydroelastic analysis to model the behavior and energy extraction of a Flexible Floating Breakwater (FFB), demonstrating its effectiveness in both coastal protection and wave energy production. Taking into account the straightforward design and the potential for advancement of pile-restrained floating breakwaters (PRFBs), Ning et al.[4] suggested incorporating a hydraulic PTO system into the PRFB. Subsequently, Ning et al.[5] conducted an analytical study on the hydrodynamic performance of a dual-pontoon WEC-type breakwater and concluded that the dual-pontoon system

Hydroelastic performance of a flexible pontoon-type floating breakwater embedded with multiple oscillating-water-column devices

outperforms the single-pontoon system in terms of transmission coefficient and effective capture width ratio. Zhao et al.[6] developed a hybrid system incorporating an OB-type WEC placed on the windward side of a breakwater. The experiments showed that, compared to the isolated setup, the WEC's capture factor was considerably enhanced when positioned in alignment with the breakwater's orientation relative to the waves. Tay[7] introduced an innovative configuration of raft-type wave energy converters (WECs) combined with a long floating breakwater and conducted a numerical study in the frequency domain. The findings indicate that the hydroelastic behavior of the floating breakwater influences the capture factor of the WECs. Cheng et al.[8] performed a numerical analysis on the wave energy capture of modular OB-type floating breakwaters placed on the wave-facing side of a large floating structure. Their results show that WECs can effectively combine energy extraction with hydroelastic mitigation.

Due to their simplicity and reliability, OWC-type wave energy converters (WECs) have garnered significant interest from researchers exploring their potential integration with floating breakwaters. Koo[9] developed a floating box breakwater featuring an air chamber in the center to create an oscillating water column (OWC) device and studied its wave attenuation capabilities. Due to the effective aerodynamic damping in dissipating wave energy, this design exhibits a lower transmission coefficient compared to traditional box-type breakwaters. Zhao et al.[10] conducted experimental comparisons of the hydrodynamic performance of OWC devices with varying chamber numbers and discovered that multi-chamber OWCs offer better capture factor. Malara and Arena[11] used a semi-analytical model based on three-dimensional linear wave theory to study hydrodynamic interactions in U-OWC arrays. Xu et al.[12] conducted wave flume experiments to investigate the effects of front-wall opening height, U-tube length, and height on U-OWC performance. Moretti et al.[13] developed a combined system featuring a floating breakwater and a U-OWC device equipped with a dielectric elastomer generator PTO, designed to harness wave energy by utilizing the large deformations of membranes. Howe et al.[14] proposed a configuration of bent duct-type OWC wave energy converters integrated into the leeward side of a floating breakwater and carried out corresponding model experiments. As a general extension, Howe et al.[15] experimentally studied the impact of breakwater motion on the hydrodynamic performance of the OWC wave energy converter, concluding that pitch motion negatively affects capture factor.

In addition, advanced theoretical, numerical, and experimental approaches have been extensively applied to simulate the hydrodynamic performance of hybrid systems that combine OWC devices with floating breakwaters.[16] Using linear potential flow theory, Zhao et al.[17] evaluated the power generation capture factor and wave reduction performance of a PRFB system through the eigenfunction matching approach. Reabroy et al.[18] investigated the asymmetric effects on the hydrodynamics of the OB WEC, taking into account the interaction between incident and reflected waves. Cheng et al.[19] found that OWC-type DPFB with non-uniform draft outperforms OB-type SPFB in wave attenuation and energy conversion. Subsequently, Cheng et al.[20] developed a nonlinear model to analyze a hybrid OB-OWC breakwater, demonstrating improved energy capture and wave attenuation through coupled resonance and efficient OB design. Martins-Rivas and Mei[21] installed OWC devices on a breakwater and analyzed their hydrodynamic performance based on nonlinear potential flow theory. Elhanafi et al.[22] used experiments and CFD modeling to assess a floating-moored OWC, finding that surge motion improves capture factor near resonance and wave height/tension affect performance. Elhanafi et al.[23] used a 3D model based on RANS equations to compare single- and dual-chamber OWC

Hydroelastic performance of a flexible pontoon-type floating breakwater embedded with multiple oscillating-water-column devices

devices, finding that dual-chamber OWCs greatly enhance energy extraction in intermediate and long waves. Tsai et al.[24] developed a 3D model to examine the effects of front wall submergence, orifice size, and porosity on a modified breakwater-integrated OWC with a perforated front wall. Zhou et al.[25] used a 3D time-domain model to study the hydrodynamic response of an OWC integrated with an OWT, validating OWC response and air pressure against experimental data. Zheng et al.[26] created a 3D analytical model to assess the capture factor of a system combining an array of OWCs with a breakwater, focusing on their synergistic interaction. Chen et al.[27] proposed a leeward inlet OWC and numerically studied key structural parameters, showing superior long-wave attenuation and notable energy capture in a four-unit array. Furthermore, Cheng et al.[28] used a coupled FVM-FEM simulation to analyze an integrated OWC-floating breakwater system, finding that energy conversion conflicts with wave attenuation, elastic deformation reduces capture factor, and gap resonance amplifies energy peaks. Integrated WECs with fixed breakwaters have been successfully applied globally, such as the 60 kW Sakata port breakwater in Japan[29], the 18.5 kW Mutriku plant in Spain[30], the 4 MW Siadar plant in Scotland[31], and a 113kW marine LIMPET project in the Scotland[32].

Recent studies have highlighted the superior adaptability of flexible structures to wave-induced loads, especially under wave–structure interaction conditions where hydroelastic deformation plays a critical role in modifying wave attenuation behavior and energy capture characteristics. Collins et al.[33] categorized flexible wave energy devices into deformable membranes, bulge wave devices, and carpet membranes. Algie et al.[34] analyzed the mWave system through numerical modeling, finding its optimal performance at a 9s wave period and an estimated annual power output of 240 kW in nearshore conditions. Smith[35] investigated a bulge wave-based converter, revealing that optimizing capture width enhances energy extraction, with predictions aligning with experimental results. Babarit et al.[36] examined the dynamic response of flexible electroactive WECs, deriving their flow evolution and vibrational modes, validated through tank experiments at École Centrale de Nantes. Ancellin et al. [37] studied the maximum absorption width of multi-degree-of-freedom WECs, applying it to SBM Offshore S3 converter, showing better performance at wavelengths shorter than the device length, suggesting larger designs for optimal capture. Deborah et al.[38] compared three inflatable WEC configurations—partially submerged, fully submerged, and bottom-fixed—demonstrating distinct dynamic behaviors, with numerical and experimental results matching well. Michele et al. [39] developed a mathematical model for flexible floating WECs, confirming that elasticity increases resonance frequencies, enhancing energy output but reducing peak capture factor in irregular waves (JONSWAP spectrum), emphasizing the need for large-scale experimental validation. Zheng et al.[40] proposed a floating elastic wave energy converter with a disk-shaped plate moored via a PTO system, showing that a continuous PTO enhances energy capture across a wide frequency range and theoretically achieves 100% absorption through optimized damping and stiffness. Zheng et al. [41] also developed a theoretical model for hydroelastic interactions between water waves and porous elastic plates, showing that wave dissipation is enhanced through hydrodynamic interactions, with applications in wave energy harvesting and flexible ice modeling. Liu et al.[42] used CFD to study a modular OWC–floating breakwater, finding that optimal stiffness and spacing enhance capture factor, while excessive flexibility causes multimode instability and efficiency loss. Teng et al.[43] developed a Computational Fluid Dynamics (CFD)–Finite Element Method (FEM) coupling approach to investigate the energy capture efficiency of a floating carpet-type wave energy converter (WEC)

equipped with an array of PTO units.

Existing studies have provided valuable insights into the design and performance analysis of WEC-integrated floating breakwater systems. In practical applications, floating breakwaters are often assembled from multiple interconnected modules to ensure sufficient shielding and wave attenuation, leading to ultra-long flexible systems. Due to their high aspect ratio in both longitudinal and transverse directions, the elastic deformation of such structures becomes a crucial factor influencing their performance. Furthermore, the inhomogeneous distribution of wave characteristics along ultra-long structures can induce significant hydroelastic responses, particularly under oblique wave incidence. To address these challenges, this study proposes a novel multi-module flexible box-type floating breakwater, embedded with multiple oscillating water column (OWC) devices, each equipped with an independent power take-off (PTO) system. The OWC chambers are arranged in a linear array along the length of the breakwater, forming an integrated wave energy conversion system. The key contributions of this study are twofold: firstly, a coupled fluid-structure hydroelastic model is developed to analyze the impact of breakwater deformation on system performance; secondly, the capture factor and wave attenuation characteristics of the integrated system are systematically evaluated through parametric analysis.

This work is arranged as follows: Section 2 introduces the establishment of a new flexible OWC-breakwater model, incorporating compressed air-water-solid interactions and the principles of rigid-flexible coupled motion. In Section 3, the validation of the developed numerical model is carried out. Section 4 introduces a parametric sensitivity analysis, primarily focusing on the optimal configuration of OWCs within the integrated system and examining the hydroelastic response of the flexible breakwater. Finally, the conclusions are summarized in Section 5.

2. Numerical method

2.1 Model establishment and numerical wave tank

In the numerical model, a very long flexible floating breakwater with a number of N chambers, possessing a bending stiffness of EI (where E denotes the elastic modulus and I is the cross-section rotational inertia), is arranged in the wave-structure interaction zone, as shown in Fig. 1, where $N=5$ is considered as an example. Each chamber is equipped with an independent Power Take-Off (PTO) wave energy conversion system. Additionally, the width of the opening at the bottom of each chamber is reduced by adding a baffle. The insert plate at the bottom of the chamber is symmetrical on the left and right sides and has the same length on both sides. The water depth defined as h is constant. The detailed model parameters are listed in Table 1. The air-water two-phase model has a total length of 7 times the incident wavelength (λ), with two damping zones, each 1.5λ in length, placed at both ends of the computational domain to absorb the reflected and transmitted waves, respectively. Velocity inlet is applied between the front damping zone and the OWC device to generate incident waves. A segregated flow model is employed for the simulations, with air compressibility in the chambers considered under the assumption of an isothermal ideal gas. Assuming isothermal conditions eliminates the need to solve an energy transport equation, thereby simplifying the simulation and reducing runtime.

Hydroelastic performance of a flexible pontoon-type floating breakwater embedded with multiple oscillating-water-column devices

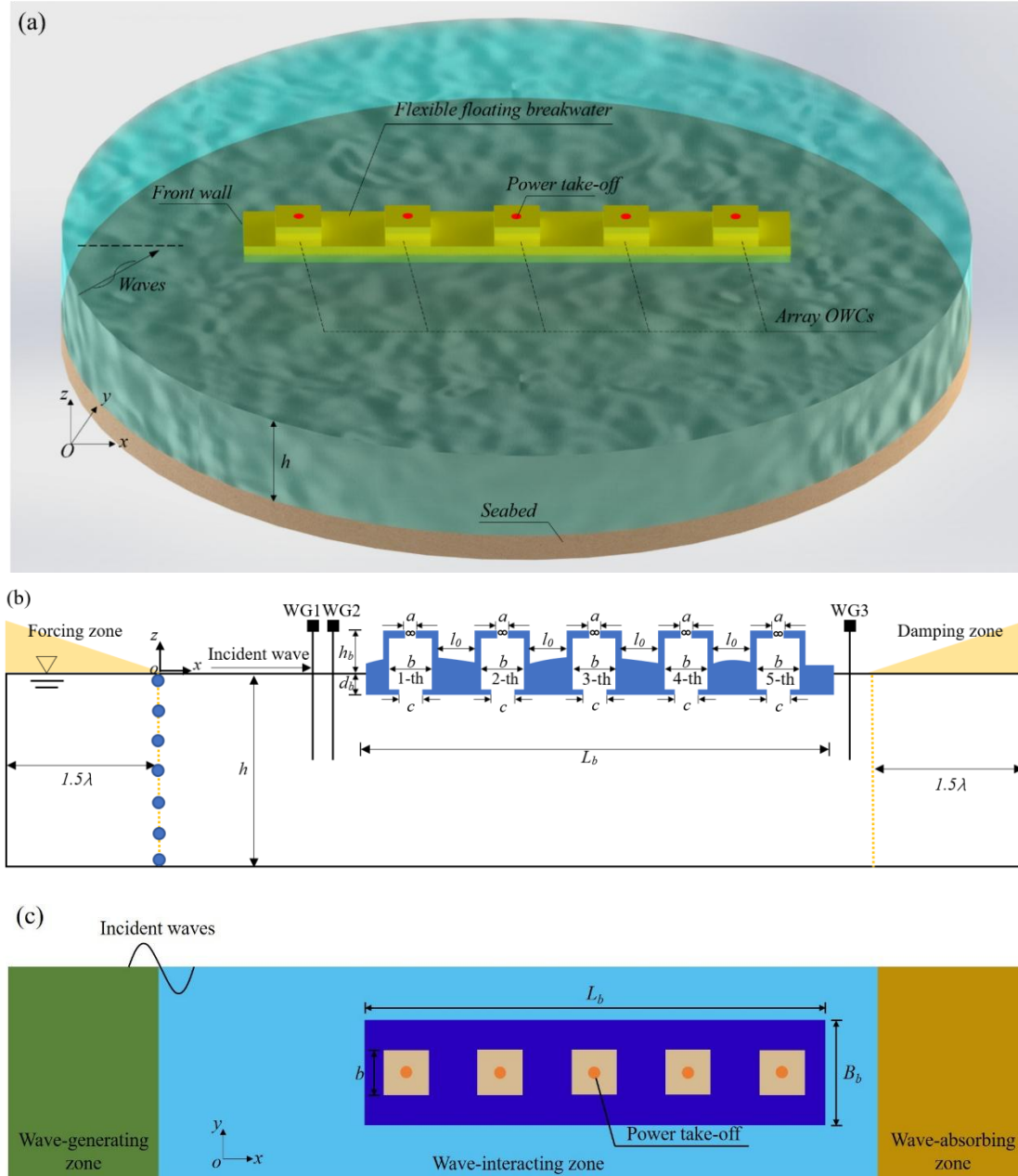


Fig. 1 A diagram of system in a 3-D wave tank (a) bird's-eye view (b) Side view (c) Top view

Table 1 Key parameters of the numerical model.

Parameters	Value
Breakwater length (L_b) [m]	60
Breakwater width (B_b) [m]	8
Chamber width (b) [m]	4
Orifice opening (a) [-]	0.00785
Length of the insert plate (c) [m]	2
Breakwater draft (d_b) [m]	1
Breakwater freeboard height (h_b) [m]	2
Water depth (h) [m]	10
Duration of the CFD simulation	10T

2.2 Mesh generation

Employing viscous CFD code, a three-dimensional numerical wave tank (NWT) is crafted to emulate the efficacy of flexible floating breakwaters. The overset mesh method offers a precise and convenient approach for handling complex free surface flows. The method partitions the free surface into overlapping sub-domains, enabling the flow within each region to be computed independently. In this study, the overset mesh method is adopted to discretize the mesh surrounding the hybrid system. A no-slip wall boundary condition is imposed on the object's surface, while the external region is defined with the overset mesh condition. To enhance the solution accuracy, a trimmed mesh model is utilized to divide the area surrounding the free surface into a liquid transition zone and a liquid encryption zone. The flexible floating breakwater is meticulously affixed at the midpoint of the NWT. The final computation typically uses a mesh containing approximately 1000,000 volume cells. The mesh within the motion zone of the system is encrypted, as depicted in Fig. 2.

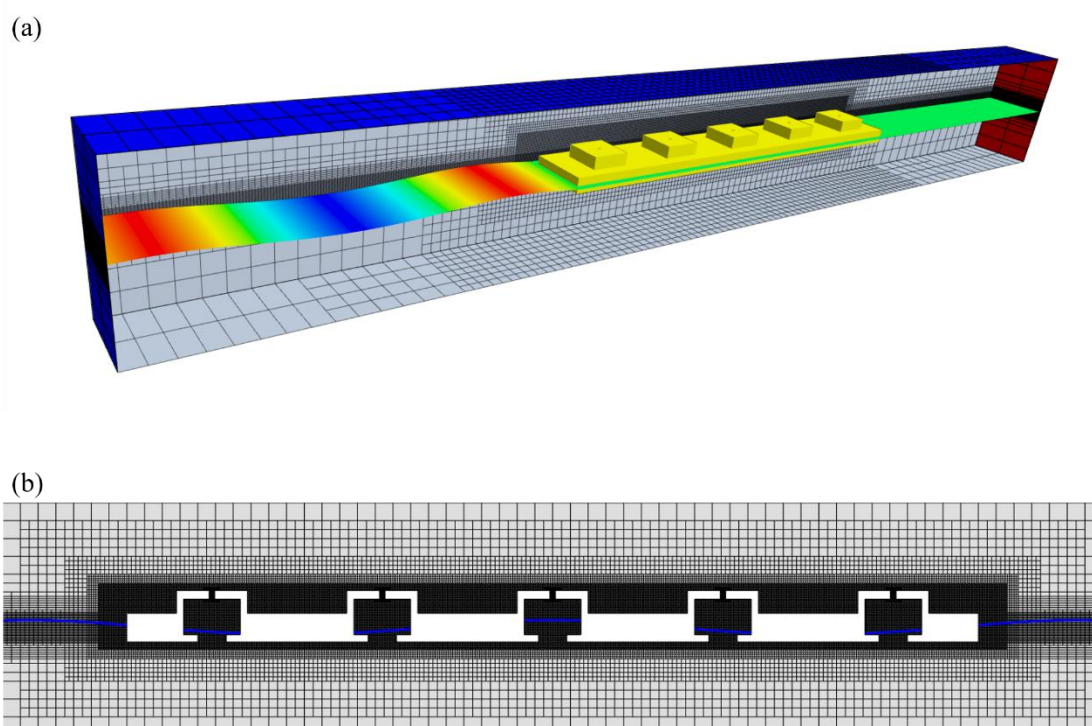


Fig. 2 (a) Typical mesh for the perimeter of the hybrid system. (b) Spatial distribution of wave profiles inside each chamber.

2.3 FSI coupling procedure

In this study, the Fluid-Structure Interaction (FSI) approach is used, which refers to a coupled surface problem in which the state of the fluid model depends on the state of the structural model, and vice versa. The FSI simulation is affected by the law that the corresponding fluid and solid particles at the coupled interface move with the same kinematic properties and are subjected to the same tensile forces. This law results in kinematic and force consistency. These two sets of coherence are used to model the interactions according to the following descriptions: first, the information transferred from the fluid to the solid is the fluid tension, which consists of the fluid pressure and

Hydroelastic performance of a flexible pontoon-type floating breakwater embedded with multiple oscillating-water-column devices

the wall shear stress, and second, the information transferred from the solid to the fluid is the deformation of the solid, in particular, the deformation at the fluid-structure interface.

2.4 Governing Equations

Fluids must adhere to the principles of mass and momentum conservation. Additionally, the change in mass within a differential volume of fluid is equal to the net mass entering that volume. The mass conservation equation is as follows:

$$\frac{\partial \rho}{\partial t} + \nabla \cdot (\rho \mathbf{u}) = 0 \quad (1)$$

where ρ refers to the fluid density, t refers to the time, $\nabla = \left(\frac{\partial}{\partial x}, \frac{\partial}{\partial y}, \frac{\partial}{\partial z} \right)$ is the differential

operator. The above equation is also known as the continuity equation. For incompressible fluids ρ is constant, and the above formula is expressed as:

$$\nabla \cdot \mathbf{u} = 0 \quad (2)$$

The conservation equation states that the rate of change of fluid momentum in the microstructure over time is equal to the total force acting on the micro body. The momentum conservation equation can be expressed as:

$$\frac{\partial (\rho \mathbf{v})}{\partial t} + \nabla \cdot (\rho \mathbf{v} \otimes \mathbf{v}) = \nabla \cdot \boldsymbol{\sigma} + \mathbf{f}_b \quad (3)$$

where \otimes refers to the outer product, \mathbf{f}_b is the resultant force of various volume forces acting on the unit volume of the continuum, $\boldsymbol{\sigma}$ is the stress tensor. For fluids, the stress tensor is usually written as the sum of normal stress and shear stress, so $\boldsymbol{\sigma} = -p\mathbf{I} + \mathbf{T}$. Among them, p is the pressure, \mathbf{T} is the viscous stress tensor, and we get:

$$\frac{\partial (\rho \mathbf{v})}{\partial t} + \nabla \cdot (\rho \mathbf{v} \otimes \mathbf{v}) = -\nabla \cdot (p\mathbf{I}) + \nabla \cdot \mathbf{T} + \mathbf{f}_b \quad (4)$$

Turbulence equations form the foundation for CFD simulations. In this study, the Eulerian multiphase flow model utilizes incompressible Reynolds-Averaged Navier-Stokes (RANS) equations to describe water-air mixtures, and the volume of fluid (VOF) method is applied to capture the interface dynamics between the air and water phases. The total mass conservation equation for all phases are given by:

$$\frac{\partial}{\partial t} \left(\int_V \rho dV \right) + \oint_A \rho \mathbf{v} \cdot d\mathbf{a} = \int_V \Omega dV \quad (5)$$

where \mathbf{a} refers to the surface area vector, \mathbf{v} is the mixture (mass-averaged) velocity, Ω is a mass source term that is related to the phase source term as follows:

$$\Omega = \sum_i \Omega_{a_i} \cdot \rho_i \quad (6)$$

The VOF wave model is employed to simulate surface gravity waves at the air-water interface. Stokes wave theory's fifth-order approximation is used to model higher-order waves, which more accurately represent real waves compared to those generated by first-order methods. Both the wave

Hydroelastic performance of a flexible pontoon-type floating breakwater embedded with multiple oscillating-water-column devices

shape and phase velocity are influenced by factors such as water depth, wave height, and current. The Ursell number U_R is defined as:

$$U_R = \frac{H\lambda^2}{h^3} \quad (7)$$

where H is the wave height, λ is the wavelength.

2.5 Wave energy conversion

The hydroelastic behavior of the floating breakwater produces multi-mode radiated waves, which influence both water oscillations and airflow within the OWC chambers. To simulate the damping effect of the PTO system, a circular orifice is placed at the top of each chamber. The air pressure p_{ai} existing inside i -th OWC chamber is expressed as

$$p_{ai} = \frac{1}{2} \rho_a C_d |U_{ai}(t)| U_{ai}(t) \quad (8)$$

where $U_{ai}(t)$ is the airflow velocity through the orifice. In the above formula, the right-hand term is the pressure drop due to the PTO, which results in the loss of air pressure. Quadratic pneumatic damping coefficient C_d is determined by

$$C_d = \left(\frac{1}{\alpha C_c} - 1 \right) \quad (9)$$

where α is the opening ratio of the orifice, which is assumed to be identical for all chambers. C_c is the shrinkage coefficient and can be approximated by taking the average value of $C_c = 0.61$ for a thin-walled circular orifice. Thus, the period-average power extraction by the i -th OWC device can be expressed as:

$$E_p = \frac{A_0}{T} \int_{t_0}^{t_0+T} \sqrt{\frac{2|P_{ai}(t)|^3}{\rho_a C_d}} dt \quad (10)$$

where E_w denotes the incident wave energy along the propagating direction perpendicular to the breakwater length and is written for regular incident waves as:

$$E_w = \frac{1}{16} \frac{\rho g H_i^2 \omega B}{k} \left(1 + \frac{2kh}{\sinh 2kh} \right) \quad (11)$$

where H_i is the incident wave height, h is the water depth, T is the wave period, B is the transverse length of the floating breakwater.

Thus, the hydrodynamic capture factor of an OWC device is calculated from

$$\zeta = \frac{E_p}{E_w} \quad (12)$$

As shown in Fig. 1 (b), three wave gauges (WG1, WG2 and WG3) are set up in the NWT, with WG1 and WG2 set up in front of the breakwater and WG3 set up behind the breakwater. To prevent the reflected and incident waves from being separated due to the same wave surface elevation measured by WG1 and WG2, the spacing between WG1 and WG2 is set to 0.1λ (λ is wavelength), and WG2 is located at a distance λ from the front end and the breakwater. The reflection coefficient

of the breakwater K_r and the transmission coefficient K_t can be expressed as

$$K_r = \frac{H_r}{H_i} \quad (13)$$

$$K_t = \frac{H_t}{H_i} \quad (14)$$

For a floating breakwater, the objective is to attenuate incident wave energy. In general, lower values of both K_r and K_t are desirable, as they indicate that a greater proportion of the wave energy is absorbed by the OWC chambers rather than being reflected or transmitted. This criterion is consistent with the aim of enhancing energy capture while reducing wave energy propagation past or back toward the structure.

3. Model Validation

3.1 Convergence study

In numerical simulations, the dynamic motion and deformation of the structure significantly affect computational accuracy. Selecting appropriate time steps and mesh parameters not only ensures the precision of the results but also optimizes computational capture factor. This study employs a simulation scenario with a wave height $H_i=1$ m, water depth $h=10$ m, and wave period T ranging from 3 s to 9 s. The wave condition with $T=5$ s was selected to verify the convergence of the long-period three-dimensional numerical wave tank simulation, and the measured wave surface elevations were compared.

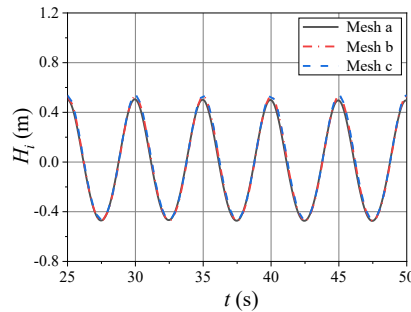


Fig. 3 Convergence of incident wave heights with different meshes.

Fig. 3 shows the wave elevation profiles before and after the structure for three different mesh schemes: Mesh a ($\Delta z=H_i/20$, $\Delta x=H_i/10$), Mesh b ($\Delta z=H_i/30$, $\Delta x=H_i/15$), and Mesh c ($\Delta z=H_i/40$, $\Delta x=H_i/20$). The results indicate that although the phase differences between the three meshes are less than 3%, significant amplitude differences are observed, particularly between Mesh b and the other two meshes, where the amplitude difference exceeds 5%. This discrepancy is likely caused by numerical dispersion due to the coarse grid of Mesh a. Moreover, the amplitude difference between Mesh b and Mesh c remains within 3%, demonstrating that Mesh b provides sufficient accuracy, while Mesh c demands significantly higher computational costs without corresponding improvements in results. After achieving time step convergence, the time step for all three mesh schemes was set to $dt=T/400$. The results show that selecting the intermediate time step $dt=T/400$ achieves an optimal balance between computational time and solution accuracy. Therefore, unless

otherwise specified, subsequent simulations will employ Mesh b and a time step of $dt=T/400$.

3.2 Comparison

To validate the numerical model, an experimental example of the seabed-sitting triple-chamber OWC device[44] is considered with the geometrical parameters as follows: $b/h=0.343$, $c/h=0.014$, $d_1/h=0.178$, $d_2/h=0.178$, $d_3/h=0.178$, $d_4/h=1.0$ and $h=0.7$ m. Fig. 4 shows the comparison of the overall hydrodynamic efficiency between the CFD numerical solutions and the reference, the good agreement suggests the current methodology is capable of accurately simulating M-OWC problems. A root mean square error (RMSE) between the numerical and experimental results is calculated to quantify the model's accuracy. A value of 0.025 in the RMSE further confirmed the suitability and accuracy of the proposed method.

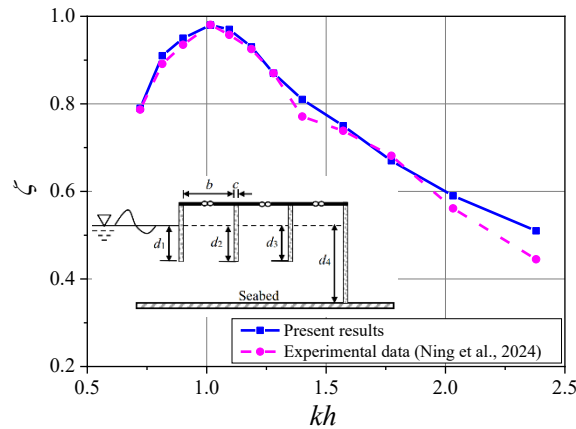


Fig. 4 Comparison of the overall hydrodynamic capture factor between numerical and experimental results for a seabed-sitting triple-chamber OWC device

Montiel et al.[45] performed a series of experiments at the Fluid Mechanics Research Laboratory of the Ecole Centrale de Nantes to study the bending response of a floating thin elastic disk to a single-frequency wave. The experiments were conducted with a wave period of $T = 0.9$ s, an incident wave height of $H_i = 0.014$ m, and a disk thickness of 10 mm. A comparison of the time-dependent deflection (corresponding to the displacement RAO in frequency-domain analyses) at the center-point between the numerical simulations and experimental results is presented in Fig. 5. The close agreement between the simulation and experimental data indicates that the proposed simulation method is capable of accurately predicting the dynamic response of structures under wave loading.

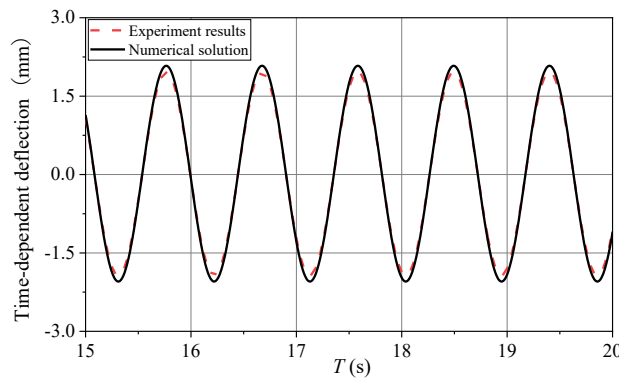


Fig. 5 Comparison of numerical and experimental deflection

4. Results and discussion

Based on the proposed FSI coupling method, the hydrodynamic performance of the long flexible floating breakwater integrated with the M-OWC is investigated, including the reflection coefficient, transmission coefficient, capture factor, hydroelastic response, and wave field around the integrated system. Unless specified, the geometrical parameters of the flexible floating breakwater are given in terms of $L_b \times B_b \times d_b = 60 \text{ m} \times 8 \text{ m} \times 1 \text{ m}$ and $EI = 7 \times 10^{16} \text{ Nm}^2$. The breakwater has a built-in OWC gas chamber number $N = 5$, a square cross-section of the chamber, a cross-section side length $b = 4 \text{ m}$, and a chamber opening of 0.785%. Wave conditions are $H_i = 1 \text{ m}$ and $h = 10 \text{ m}$. In this paper, a dimensionless period range of 2.97-8.91 is chosen because in this range, the M-OWC has a better energy conversion than the other period ranges and it is easier to analyze devices hydrodynamic performance. First, using the established numerical model, the hydroelastic response characteristics of floating breakwaters with different stiffnesses were analyzed based on the capture factor, reflection coefficient, and transmission coefficient. Subsequently, the effects of chamber size, number of chambers, and chamber spacing on the hydrodynamic performance of the flexible floating breakwater were investigated. Finally, the influence of the presence and size of the bottom opening on the hydrodynamic performance of the breakwater was evaluated through a comparative analysis.

4.1. Effect of different stiffnesses

In this subsection, the multimode resonance characteristics of the M-OWC flexible floating breakwater with different stiffness values are investigated. Three cases are considered, with bending stiffness $EI = 7 \times 10^{14} \text{ Nm}^2$, $7 \times 10^{16} \text{ Nm}^2$, and $7 \times 10^{22} \text{ Nm}^2$, respectively. The corresponding results for the transmission coefficient (K_t), reflection coefficient (K_r), and total capture factors are presented in Fig. 6 (a)-(c). As shown in Fig. 6 (a), the stiffness of the M-OWC flexible floating breakwater has a significant impact on the transmission coefficient within the simulated wave period range. Specifically, the transmission coefficient decreases as the breakwater stiffness increases, particularly in the medium and long wave periods. This phenomenon is likely due to the generation of multiple radiated wave modes caused by the deflection of the flexible breakwater, indicating that the structure exhibits multiple resonance modes. The fundamental mode corresponds to the rigid undulating motion, while the higher-order modes arise from the flexural stiffness of the structure. A more flexible breakwater follows wave motion more closely, leading to a greater number of radiated wave components. As seen in Fig. 6 (b), the reflection coefficient shows an inverse trend compared to the transmission coefficient: as the stiffness increases, wave transmission decreases while reflection increases. The reflection coefficient increases with greater breakwater stiffness. Notably, at $T(g/h)^{0.5}=4.0$, the stiffest and semi-flexible breakwaters exhibit lower reflection coefficients, which is attributed to the resonance of the OWC air chamber embedded in the flexible breakwater, allowing waves to be more effectively absorbed. In summary, a stiffer flexible breakwater demonstrates improved wave dissipation performance and achieves more consistent energy capture efficiency across a wider range of wave periods. This contrasting behavior between K_r and K_t is physically reasonable, as increased structural stiffness enhances wave resistance, reflecting more wave energy and allowing less transmission. However, due to hydroelastic deformation, the flexible structures tend to radiate energy through multiple modes rather than reflecting it directly, leading to

lower K_r despite higher wave motion.

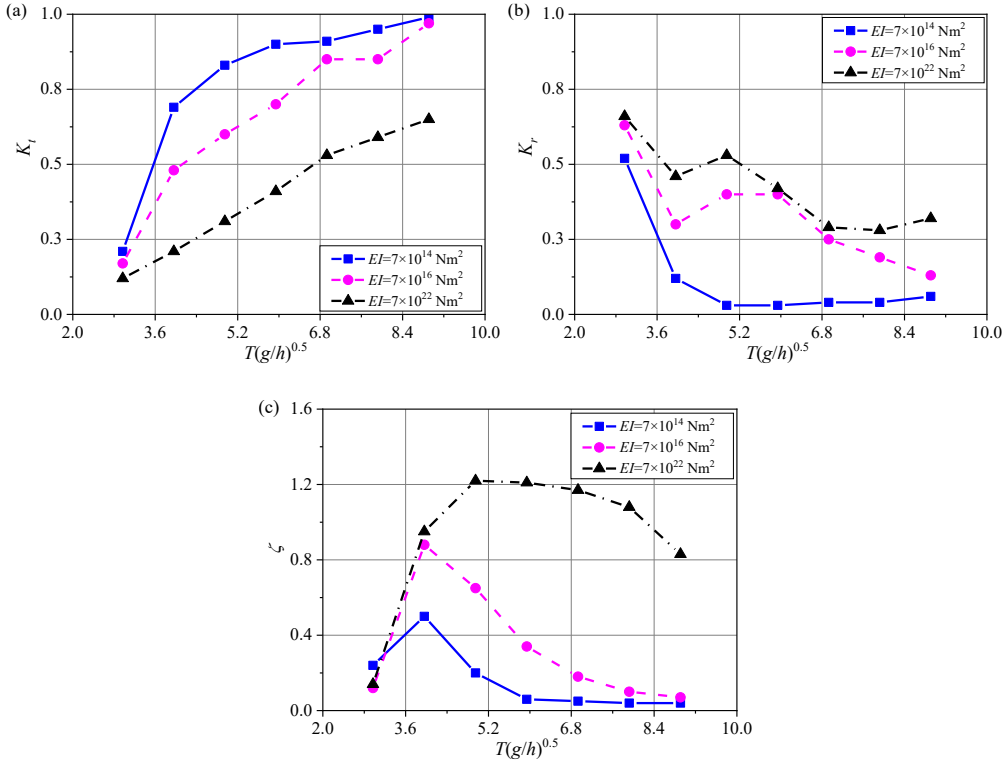


Fig. 6 Variation of (a) transmission coefficient, (b) reflection coefficient and (c) capture factor of the overall system with wave periods for different stiffnesses.

4.2. Effect of OWC chamber size

In this subsection, three different OWC chamber sizes are considered, corresponding to chamber cross-sectional side length ratios of $b/h = 0.3, 0.4,$ and 0.5 . The corresponding transmission coefficients, reflection coefficients, and capture factors as functions of the dimensionless wave period $T(g/h)^{0.5}$ are shown in Fig. 7 (a)-(c). As seen in Fig. 7 (a), the chamber size has a relatively minor effect on the transmission coefficient within the simulated wave period range when the breakwater stiffness remains unchanged. This is because the stiffness of the breakwater's main body primarily dictates the transmission coefficient, which decreases as the chamber cross-sectional side length increases. In Fig. 7 (b), it is noteworthy that, for most wave periods except within the range of $3.0 < T(g/h)^{0.5} < 5.0$, the reflection coefficient decreases as the chamber space increases. This occurs because a wider chamber allows more wave energy to enter the structure, reducing the energy reflected at the surface. Additionally, a larger chamber promotes stronger internal water-air resonance, which leads to enhanced energy absorption and less direct reflection. This wave energy redirection is particularly evident within the range $3.0 < T(g/h)^{0.5} < 5.0$, where chamber resonance plays a dominant role in modulating the wave response. As observed in Fig. 7 (c), a larger chamber has a constructive effect on the capture factor for certain wave conditions. Notably, a peak in the capture factor is observed around $T(g/h)^{0.5} = 3.9$, which corresponds to the resonance condition of the OWC chamber. In this regime, energy capture is dominated by resonance-driven air-water oscillation. Outside this range, energy capture is primarily governed by excitation force exerted by incident waves. From a coastal protection perspective, increasing the width of the breakwater along the wave propagation direction reduces the transmission coefficient. Therefore, a flexible floating

Hydroelastic performance of a flexible pontoon-type floating breakwater embedded with multiple oscillating-water-column devices

breakwater with multiple OWC modules (M-OWC) and a larger width is a more effective solution.

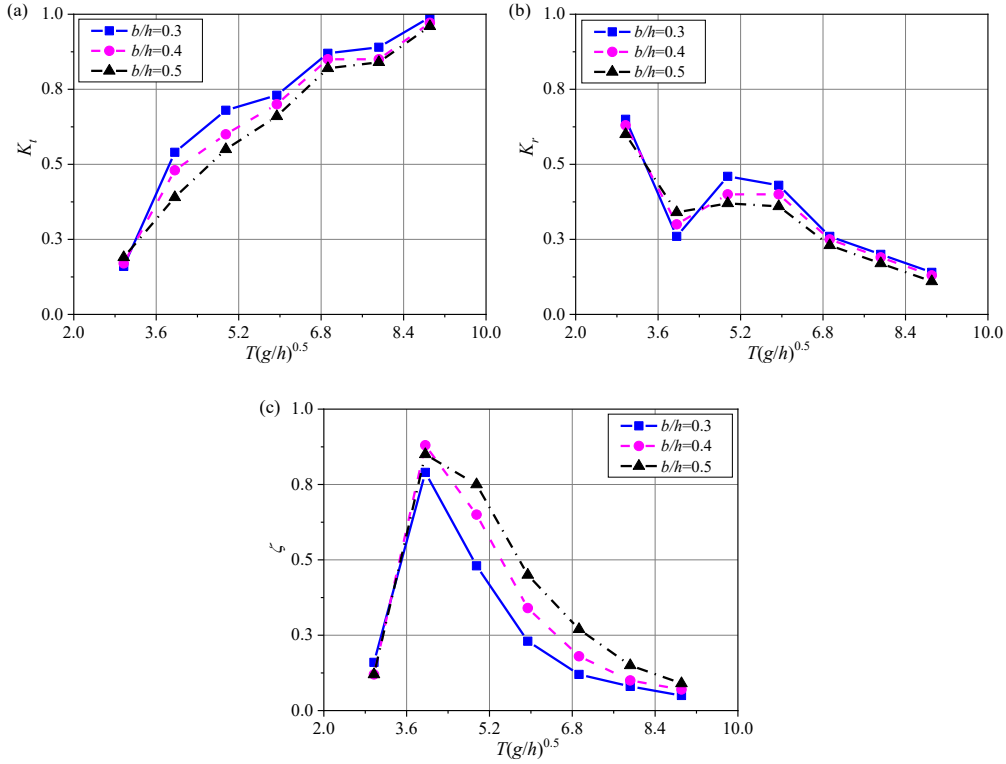


Fig. 7 Variation of (a) transmission coefficient, (b) reflection coefficient and (c) capture factor of the overall system with wave periods for different chamber size.

4.3. Effect of different chamber numbers

In this subsection, different numbers of OWC chambers are considered, i.e., $N = 3, 4,$ and 5 . In addition, Fig. 8 (a)-(c) demonstrate the distribution of hydrodynamic capture factors of individual chambers. From the capture factor plots of different numbers of OWC chambers, it can be found that when $T(g/h)^{0.5} = 2.97$, the capture factor of the foremost chamber 1 is the largest, and the capture factor of the later chambers gradually decreases. This is due to the fact that in the face of short period waves, most of the waves will be reflected by the wall. In the case of long period waves ($6.93 < T(g/h)^{0.5} < 8.91$), the energy absorption of the frontmost chamber 1 and the rearmost chamber performs better, which is mainly due to the fact that the wave capacity of the long period waves can pass through the flexible floating breakwater more easily. Therefore, the effective energy capture period of the M-OWC system is concentrated under medium period waves ($3.96 < T(g/h)^{0.5} < 6.93$), and the capture factor of the middle-most chamber tends to be the largest under medium-period resonance conditions. Meanwhile, during short-period waves, the energy capture is highest at the frontmost chamber due to direct wave reflection, while during long-period waves, the rearmost chamber performs best as waves pass through and excite it more efficiently. This spatial distribution pattern aligns with the multimodal resonance cycle, reflecting a shift from excitation-dominated to resonance-dominated capture mechanisms. However, in the flexible floating breakwater, the effective energy capture bandwidths of the chambers vary, with the front, center, and rear chambers achieving peak capture factors at short, medium, and long wave periods, respectively, aligning with the previously proposed multimode resonance cycle design.

Hydroelastic performance of a flexible pontoon-type floating breakwater embedded with multiple oscillating-water-column devices

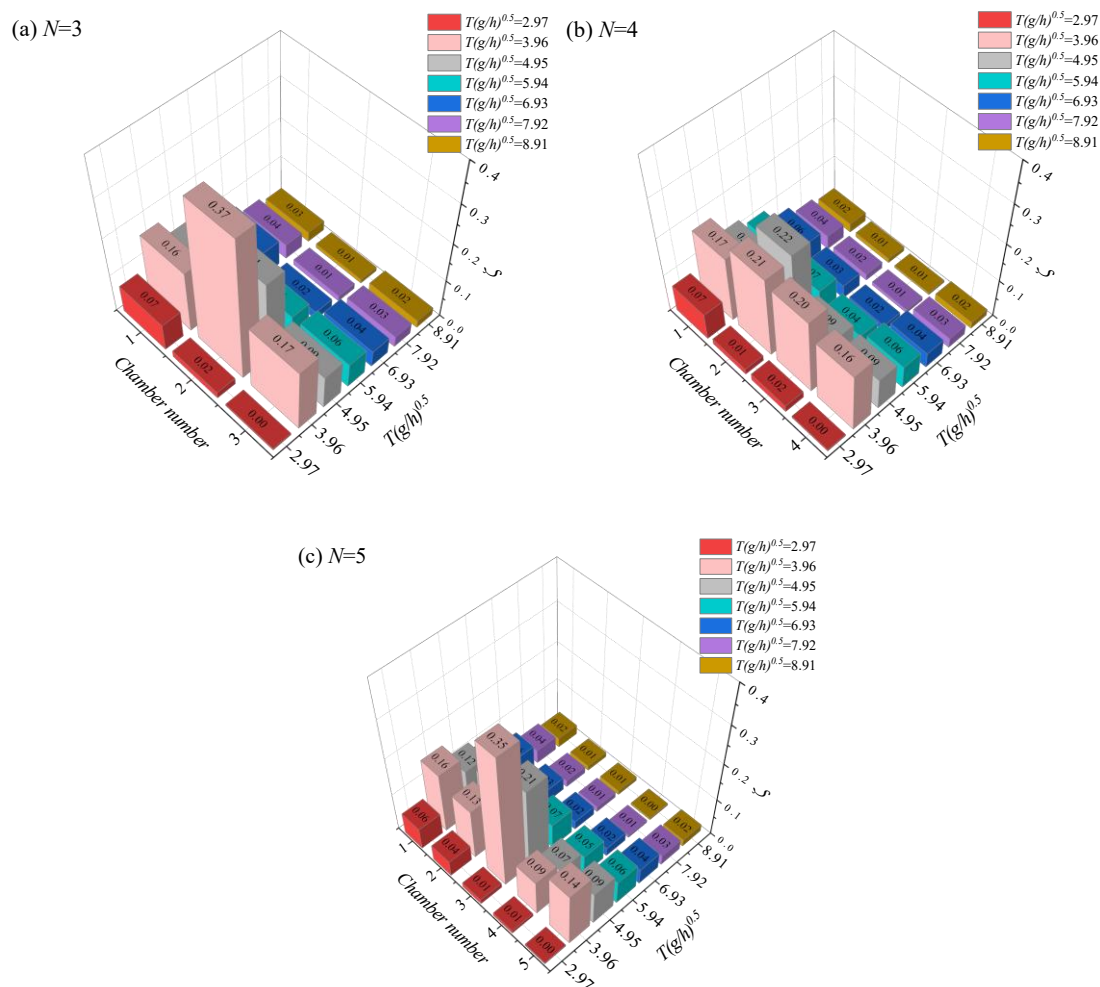


Fig. 8 Variation of the capture factor of (a) $N=3$, (b) $N=4$, and (c) $N=5$ with wave periods for different chamber numbers

Fig. 9 (a)-(b) show the comparison of different numbers of OWC chambers in terms of transmission and reflection coefficients. From Fig. 9 (a), it can be seen that the effect of different designs of the number of OWC chambers on the transmission coefficient in the multimode resonance cycle range is not significant, and the variation of the transmission coefficient with the increase of the number of chambers is not obvious. In the short wave cycle range, most of the waves are reflected by the front wall of the breakwater, while in the long wave cycle range, the transmission coefficient is relatively large, which is due to the fact that most of the waves are more likely to pass through the flexible breakwater. Therefore, in the medium wave period, the transmission coefficient decreases with the increase of the number of OWC chambers, which is due to the fact that the increase in the number of chambers inevitably absorbs more waves into the chambers. However, from Fig. 9 (b), it can be seen that the reflection coefficient decreases with increasing period in the range of $2.97 < T(g/h)^{0.5} < 3.96$, but increases slightly in the medium-long wave period ($T(g/h)^{0.5} > 3.96$). This phenomenon is attributed to the enhanced resonance response of the embedded OWC chambers under short wave periods, which promotes greater wave energy absorption and consequently reduces the reflection coefficient. However, the corresponding decrease in the transmission coefficient is not as significant, likely due to partial energy dissipation and entrapment within the chambers. As a result, the effect of resonance is more prominently

Hydroelastic performance of a flexible pontoon-type floating breakwater embedded with multiple oscillating-water-column devices

reflected in the reduction of K_r rather than K_t , particularly near the resonance period $T(g/h)^{0.5} = 3.96$.

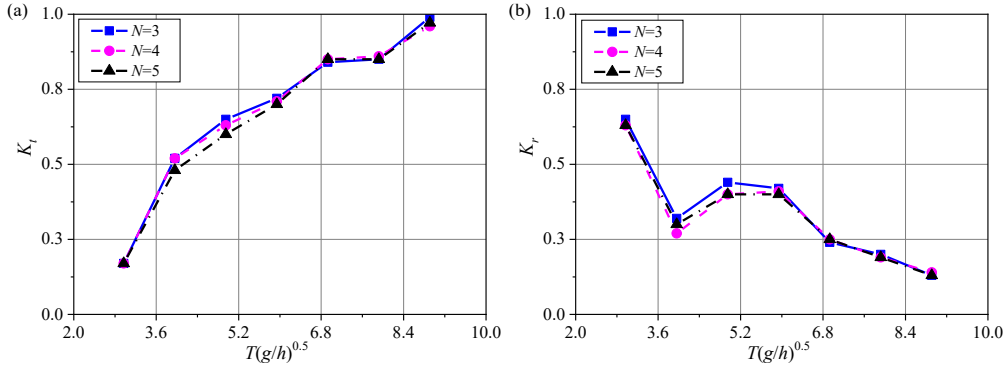


Fig. 9 Variation of (a) transmission coefficient and (b) reflection coefficient with wave periods for different chamber numbers.

4.4. Effect of OWC chamber spacing

In this subsection, the effect of OWC chamber spacing on the hydrodynamic performance of the flexible floating breakwater is considered, i.e., when $N = 3$, $l_0/h = 2.4, 2.0$ and 0.8 , and the chamber spacing is based on the chamber at the center of the breakwater. In addition, Fig. 10 (a)-(c) demonstrate the variation of transmission coefficient, reflection coefficient, and chamber capture factor with dimensionless wave period $T(g/h)^{0.5}$ for different OWC chamber spacings. From Fig. 10 (a), it can be seen that the design of the M-OWC flexible floating breakwater with different chamber spacing has less effect on the transmission coefficients in the simulated short wave period range ($2.97 < T(g/h)^{0.5} < 5.94$), whereas the effect of the transmission coefficients is more pronounced in the medium and long wave period range ($5.94 < T(g/h)^{0.5} < 8.91$). This is due to the fact that under the long wave period, the chambers at different positions will have different degrees of wave destruction and absorption, the long spaced chambers will have wave absorption at the two wave peaks, resulting in smaller transmission coefficients, while the short spaced chambers will have more pronounced wave-following in the face of the medium-long wave period, resulting in larger transmission coefficients. From Fig. 10 (b), it can be seen that the reflection coefficient decreases with decreasing chamber spacing for the simulated wave period range, this is because when the chamber spacing decreases, the body of the flexible breakwater becomes the main cause of wave obstruction, and the smaller the chamber spacing, the more concentrated the chamber location is, and the more the water resonance inside the chamber will be better, thus further decreasing the wave reflection. From Fig. 10 (c), it can be seen that for the simulated short wave period range ($2.97 < T(g/h)^{0.5} < 5.94$), the smaller spacing of the chambers has a constructive effect on the capture factor of the flexible breakwater. It is not surprising that, in the presence of short wave periods, increasing the spacing between chambers weakens the wave dissipation effect caused by concentrated wave absorption. This occurs because the main body of the flexible breakwater exhibits significant wave-following behavior, moving up and down with the waves. When the chamber spacing is reduced, the chambers become more closely positioned, enhancing the localized wave absorption effect, which leads to a higher capture factor for wave energy conversion. In contrast, under long wave periods, the traveling wave extends across the entire flexible breakwater, and narrow chamber spacing becomes less effective for long-period wave absorption. In this case, increasing the chamber spacing improves wave absorption efficiency, making it more favorable for

Hydroelastic performance of a flexible pontoon-type floating breakwater embedded with multiple oscillating-water-column devices

long-wave energy conversion.

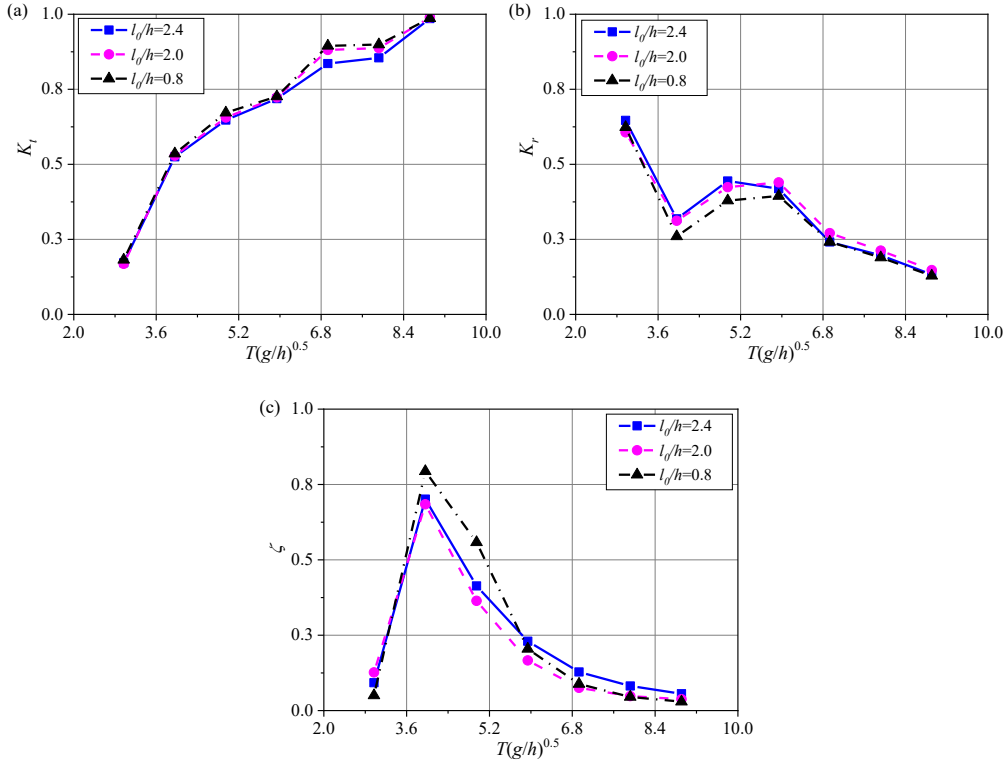


Fig. 10 Variation of (a) transmission coefficient, (b) reflection coefficient and (c) capture factor of the overall system with wave periods for different chamber spacing.

4.5. Influence of bottom opening

In this subsection, the influence of bottom opening on the hydrodynamic performance of the flexible floating breakwater is investigated, considering $c/h = 0.4, 0.3, 0.2,$ and 0.1 . The corresponding variations in transmission coefficients, reflection coefficients, and chamber capture factors with respect to the dimensionless wave period are presented in Fig. 11 (a)-(c). As shown in Fig. 11 (a), the bottom opening length has a more pronounced effect on the transmission coefficient within the simulated short wave period range ($2.97 < T(g/h)^{0.5} < 5.94$), whereas its influence is relatively minor for medium and long wave periods ($5.94 < T(g/h)^{0.5} < 8.91$). Notably, at $T(g/h)^{0.5} = 3.96$, a shorter bottom opening results in a lower transmission coefficient, primarily due to enhanced chamber resonance under short-wave conditions. This resonance promotes oscillatory motion of the water column and facilitates greater wave energy absorption, rather than merely relying on geometric openness. Conversely, a longer bottom opening improves the hydrodynamic continuity of the flexible breakwater, allowing the internal water column to oscillate more synchronously with the incident waves. This smoother interaction reduces wave reflection but also decreases the ability to trap and dissipate wave energy, thereby leading to higher transmission. As depicted in Fig. 11 (b), the reflection coefficient decreases as the bottom opening length increases at $T(g/h)^{0.5} = 3.96$. This suggests that a longer bottom opening enhances the integration of the chamber with the flexible breakwater, allowing it to move more smoothly with the wave motion. As a result, wave reflection is further reduced, which means that the breakwater interacts more efficiently with the incoming waves, minimizing energy loss through reflection and allowing greater absorption. From Fig. 11 (c), it is evident that, within the short wave period range ($2.97 < T(g/h)^{0.5} < 5.94$), the bottom opening

Hydroelastic performance of a flexible pontoon-type floating breakwater embedded with multiple oscillating-water-column devices

length significantly influences the capture factor of the flexible breakwater. Specifically, at $T(g/h)^{0.5} = 2.97$, shorter bottom openings yield higher capture factors because they direct more wave energy into the chamber, resulting in stronger pressure fluctuations and enhanced energy conversion. However, effective wave energy extraction requires both sufficient water ingress to drive air oscillations and adequate air compression. Our results indicate that intermediate opening lengths (e.g., $c/h = 0.2-0.3$) achieve the best trade-off: they allow adequate wave entry while maintaining favorable compressibility. However, for $3.96 < T(g/h)^{0.5} < 4.95$, the enhanced resonance effect associated with these intermediate openings amplifies energy capture, whereas excessively long openings limit wave inflow, reducing oscillating water column amplitude and overall efficiency. For long wave periods ($5.94 < T(g/h)^{0.5} < 8.91$), increasing the bottom opening length provides a clear advantage. Under long-period wave conditions, a longer bottom opening facilitates the formation of narrow slit resonance, which plays a key role in improving energy capture efficiency. This phenomenon enhances wave energy conversion by reinforcing the dynamic interaction between the chamber and the surrounding wave field, allowing for greater energy absorption over an extended range of wave periods.

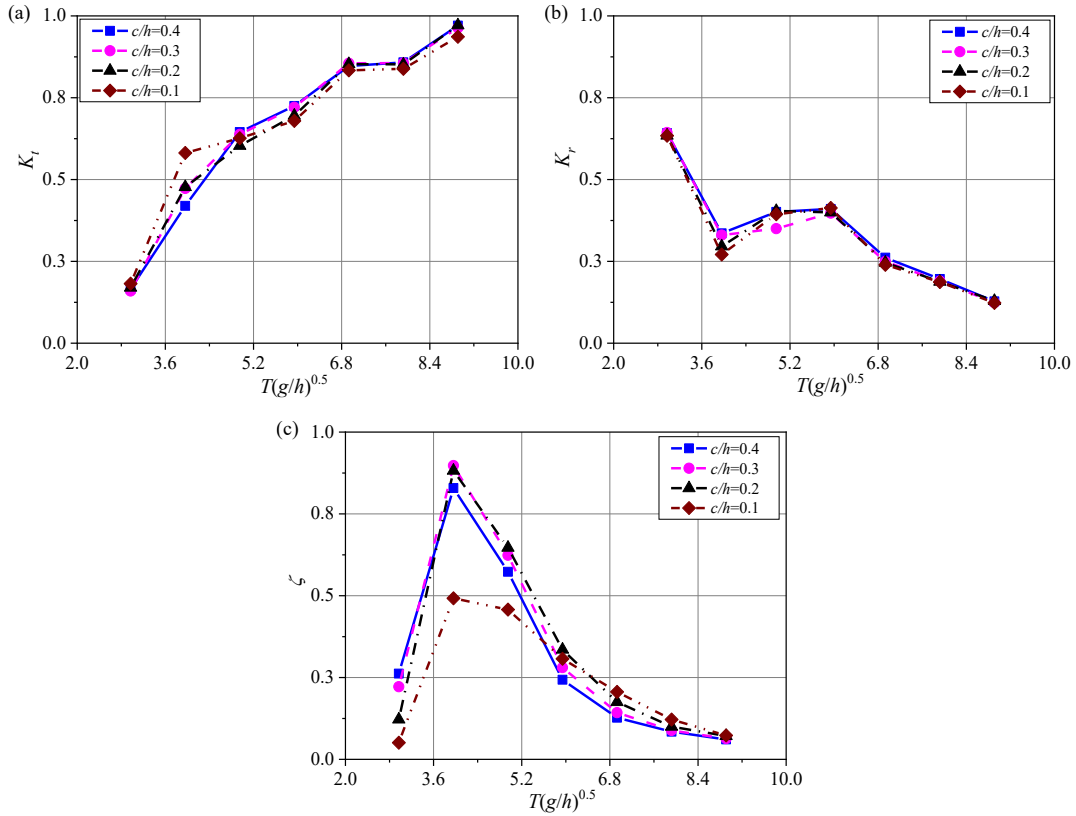


Fig. 11 Variation of (a) transmission coefficient, (b) reflection coefficient and (c) capture factor of the overall system with wave periods for different insert lengths.

Under different bottom opening conditions, the vortex field distribution is influenced by fluid shear effects, the deformation of the flexible structure, and wave-structure interactions. Unlike rigid structures, the dynamic deformation of a flexible floating breakwater under wave action leads to vortex formation, shedding, and variations in energy dissipation. For larger bottom openings (Fig. 12 (a) and (b)), water flows more smoothly, resulting in weaker shear effects, lower local vorticity, and a higher capture factor, but reduced wave attenuation capacity. In contrast, smaller bottom openings (Fig. 12 (c) and (d)) restrict fluid flow, enhancing shear layers and intensifying vortex

Hydroelastic performance of a flexible pontoon-type floating breakwater embedded with multiple oscillating-water-column devices

formation, which improves wave attenuation but may lead to excessive energy dissipation, thereby reducing the capture factor. Moreover, the impact of structural deformation on the vortex field varies depending on the bottom opening size. Larger bottom openings result in weaker interactions between structural deformation and the surrounding flow, leading to a more stable vortex distribution. Conversely, smaller bottom openings create localized high-shear regions, inducing stronger periodic vortex shedding due to restricted flow dynamics. Additionally, the deformation of the flexible structure may alter the fluid resonance effects inside the chambers, enhancing either the capture factor or wave attenuation capability depending on specific conditions. Thus, the vortex field in a flexible floating breakwater is not solely determined by the bottom opening size but also significantly influenced by the structure's dynamic response. The optimal bottom opening size should be selected based on a comprehensive evaluation of vortex intensity, shear layer stability, and the capture factor to achieve the desired balance between wave attenuation and energy capture.

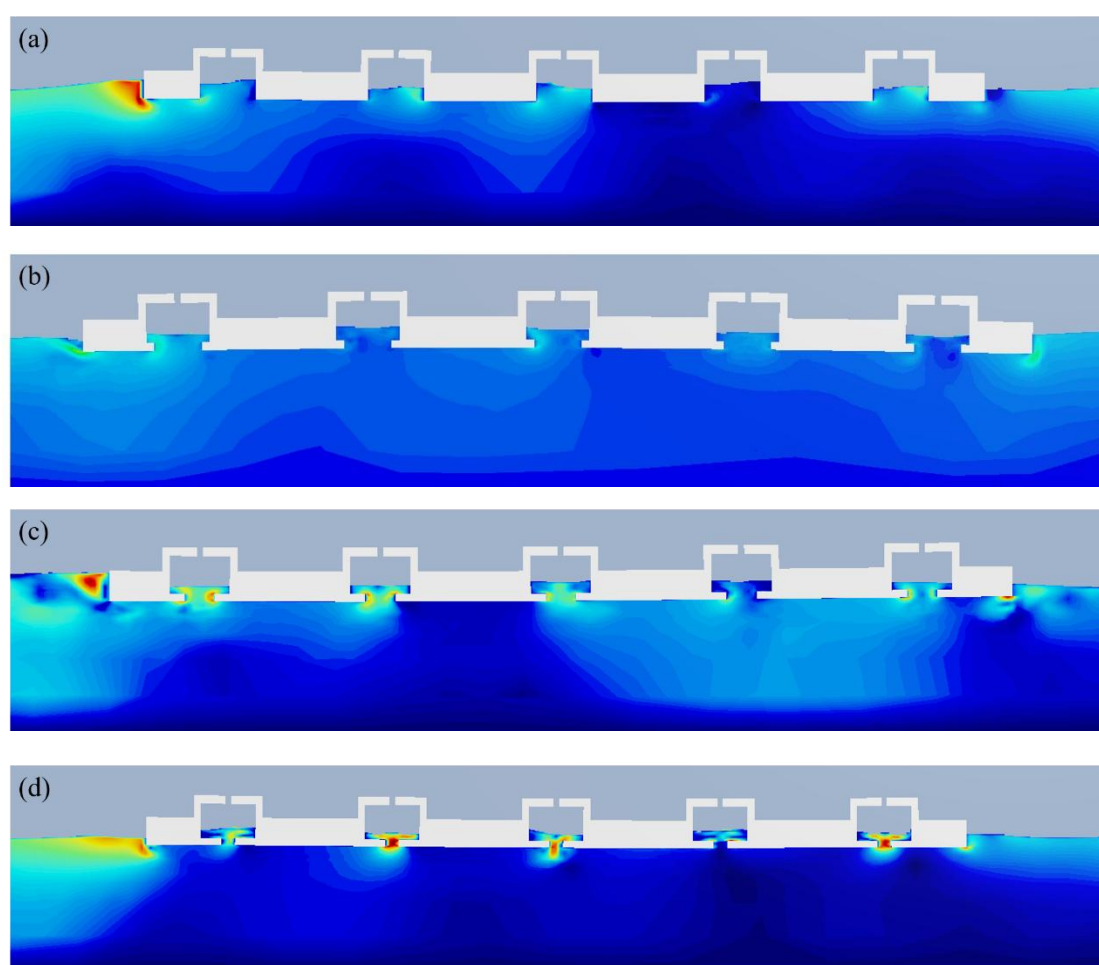
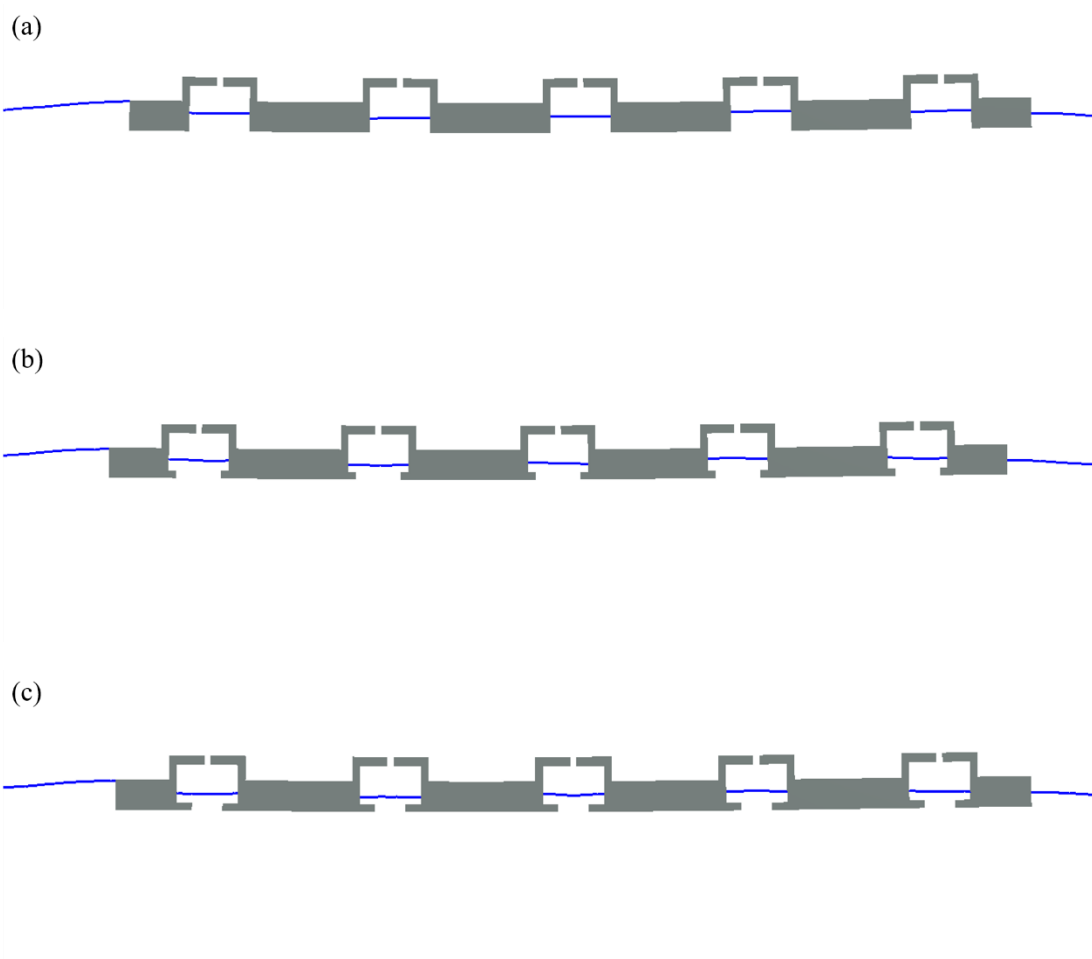


Fig. 12 Comparison of the steady vortex field around different bottom openings: (a) $c/h=0.4$, (b) $c/h=0.3$, (c) $c/h=0.2$, (d) $c/h=0.1$

Fig. 13 (a)-(d) exhibit the free surface spatial distribution for different bottom openings when the wave elevation at the front-most position reaches the maximum. The bottom opening size gradually decreases from (a) largest to (d) smallest, significantly influencing both the wave motion inside the chambers and the hydroelastic deformation of the flexible structure. In Fig. 13 (a), where the bottom opening is the largest, more wave energy enters the chambers, resulting in pronounced internal free surface oscillations. The structure exhibits relatively uniform deformation, with less

Hydroelastic performance of a flexible pontoon-type floating breakwater embedded with multiple oscillating-water-column devices

constraint on the chamber walls. However, wave attenuation is weaker as more energy passes through the openings. As the bottom opening decreases from (b) to (d), the wave height inside the chambers reduces, indicating that less wave energy penetrates into the chambers. In Fig. 13 (b) and (c), the structure shows increased localized hydroelastic deformation, particularly in the middle chambers, suggesting a stronger interaction between the flexible breakwater and wave-induced forces. In Fig. 13 (d), where the bottom opening is the smallest, the internal wave motion is highly suppressed, leading to a more stable free surface inside the chambers. The flexible breakwater exhibits greater overall bending deformation, especially in the central region, indicating that the structure's hydroelastic response is enhanced as the bottom opening decreases. Overall, the bottom opening size significantly affects both wave energy capture and structural deformation. Larger openings allow for greater energy input and internal wave motion but reduce wave attenuation effectiveness, whereas smaller openings enhance wave dissipation and hydroelastic interaction but may reduce wave energy capture efficiency inside the chambers. These observations demonstrate that the bottom opening size significantly influences not only wave energy capture but also the structural deformation characteristics along the breakwater's centerline.



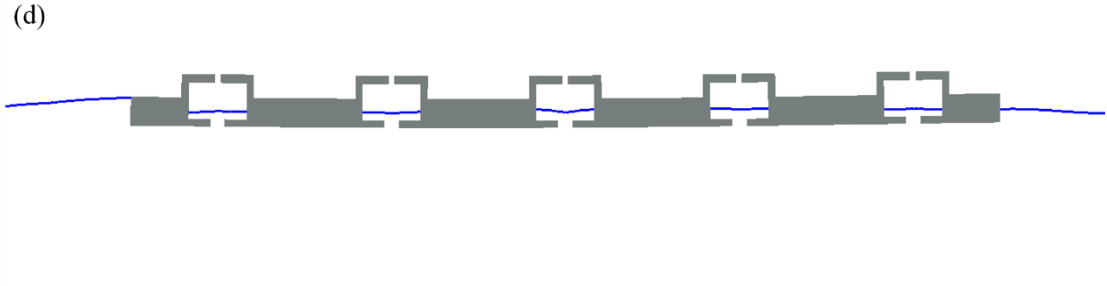


Fig. 13 Spatial distribution of wave profiles for different bottom openings when the wave elevation at the front-most position reaches its maximum

Fig. 14 (a)-(b) show that the deflection amplitude distributions along the side edge and the centreline exhibit an identical shape, both presenting a shallow “U” profile. However, the amplitude increases as the bottom opening ratio decrease. This systematic yet relatively minor variation becomes more evident near the central chambers, where smaller bottom openings enhance the hydroelastic coupling between the OWC chambers and the supporting structure, thereby amplifying localized bending responses. Conversely, larger openings attenuate this coupling, leading to a slight reduction in the overall deflection amplitudes. Thus, while the spatial distribution profile of deflection remains essentially unchanged, its magnitude is strongly dependent on the bottom opening ratio, with smaller openings producing more pronounced structural deformations.

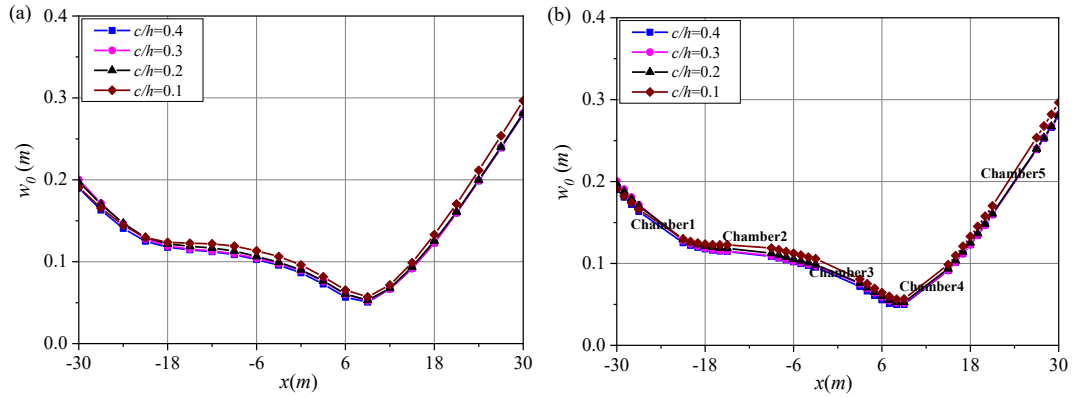


Fig. 14 Deflection amplitude distribution of the flexible floating breakwater along the length direction at $T(g/h)^{0.5}=4.95$.

5. Conclusions

Flexible floating breakwater systems with extra-long dimensions are more suitable for providing adequate shielding areas and protecting coastal infrastructure. In this work, the wave energy absorption by multiple OWCs integrated with a long-flexible floating breakwater is investigated. A coupled FSI numerical model is developed to solve the hydroelastic problem, which fully considers the deflection of the flexible floating breakwater to match the flow field information in real time.

The numerical model successfully resolves both the dynamic wave field and the structure’s deformation, especially under long-period waves where hydroelastic effects dominate. In this study, several parameter configurations were identified as favorable for enhancing wave energy capture efficiency while suppressing transmission and reflection. Specifically, a chamber width ratio of $b/h = 0.4$ balances wave entry and internal air–water oscillation; using 4 to 5 OWC chambers allows for

Hydroelastic performance of a flexible pontoon-type floating breakwater embedded with multiple oscillating-water-column devices

spatially distributed energy extraction and excitation of multimodal resonance; a chamber spacing ratio of $l_0/h = 2.0$ promotes constructive wave–structure coupling; and a bottom opening ratio of $c/h = 0.2 \sim 0.3$ offers an effective trade-off between sufficient water inflow and strong air compression. These findings provide practical guidance for the preliminary design and optimization of flexible OWC-integrated breakwater systems. The results of the study can be summarized as follows:

Enhancing the structural stiffness of multi-module flexible breakwaters proves to be an effective strategy for improving wave energy capture performance. By mitigating hydroelastic deformation, higher stiffness enables more stable internal wave dynamics and stronger chamber resonance, resulting in a consistently higher capture factor across varying wave conditions.

Moderately increasing the width of the OWC chambers along the wave propagation direction facilitates greater wave energy entry and strengthens internal resonance, thereby effectively reducing the transmission coefficient and enhancing the capture factor. Larger chamber sizes are more advantageous for improving energy conversion efficiency and wave attenuation capability over a broader range of wave periods.

Capture factor optimization requires prioritizing the foremost chamber under short-period waves through enhanced reflection, and maximizing central chamber performance under medium-period waves by leveraging hydroelastic deformation. Long-period wave absorption benefits from structural flexibility at the frontmost and rearmost chambers, validating multimode resonance design strategies.

Compact OWC arrangement near the center enhances capture factor under short-period waves due to stronger hydroelastic interactions, whereas wider spacing toward the ends favors long-period wave absorption through structural bending effects.

Incorporating a bottom opening strengthens wave resonance within the chamber, thereby increasing energy dissipation. Under long-period wave conditions, appropriately extending the opening length substantially enhances chamber capture factor.

The present study demonstrates the effectiveness of the proposed multi-module flexible pontoon-type floating breakwater under regular wave conditions using numerical simulations. The vortex field generated by fluid viscosity is clearly captured around the multi-chamber system. Although the flexible structure shows promising wave attenuation and energy capture performance, there remains a performance gap when compared to its rigid counterpart. However, complete rigidity is impractical for large-scale floating platforms, where hydroelastic deformation is often unavoidable. Therefore, this study provides valuable insight into the behavior of flexible systems and sets the stage for further enhancement. In future work, we will focus on improving energy capture by constraining hydroelastic deformation through structural optimization and the integration of PTO-based control mechanisms. Moreover, considering the prevalence of multi-directional waves in real sea states, we plan to extend the investigation to oblique wave incidence by employing a circular domain, which is more suitable for accurately simulating multi-directional wave propagation. This will allow a more comprehensive evaluation of the breakwater's applicability in realistic marine environments.

CRedit authorship contribution statement

Yinong Hu: Validation, Formal analysis, Writing-original draft, Investigation. **Yong Cheng:** Methodology, Software, Data curation, Writing-original draft, Supervision. **Saishuai Dai:** Formal analysis, Data curation, Writing-review & editing, Supervision. **Zhiming Yuan:** Writing-review & editing. **Atilla Incecik:** Supervision.

Declaration of Competing Interest

The authors declare that they have no known competing financial interests or personal relationships that could have appeared to influence the work reported in this paper.

Acknowledgment

The authors are grateful to the National Natural Science Foundation of China (Grant No. 52271278, 52111530137), National Key Research and Development Program (2024YFD2400804), the Natural Science Found of Jiangsu province (Grant No. BK20241015), and the Newton Advanced Fellowships (Grant No. NAF\R1\180304) by the Royal Society for supporting this work.

References

- [1] Abhinav KA, Collu M, Benjamins S, Cai H, Hughes A, Jiang B, et al. Offshore multi-purpose platforms for a Blue Growth: A technological, environmental and socio-economic review. *Science of The Total Environment*. 2020;734.
- [2] Mustapa MA, Yaakob OB, Ahmed YM, Rheem C-K, Koh KK, Adnan FA. Wave energy device and breakwater integration: A review. *Renewable and Sustainable Energy Reviews*. 2017;77:43-58.
- [3] Michailides C, Angelides DC. Modeling of energy extraction and behavior of a Flexible Floating Breakwater. *Applied Ocean Research*. 2012;35:77-94.
- [4] Ning D, Zhao X, Götteman M, Kang H. Hydrodynamic performance of a pile-restrained WEC-type floating breakwater: An experimental study. *Renewable Energy*. 2016;95:531-41.
- [5] Ning D-Z, Zhao X-L, Zhao M, Hann M, Kang H-G. Analytical investigation of hydrodynamic performance of a dual pontoon WEC-type breakwater. *Applied Ocean Research*. 2017;65:102-11.
- [6] Zhao X, Ning D. Experimental investigation of breakwater-type WEC composed of both stationary and floating pontoons. *Energy*. 2018;155:226-33.
- [7] Tay ZY. Performance and wave impact of an integrated multi-raft wave energy converter with floating breakwater for tropical climate. *Ocean Engineering*. 2020;218.
- [8] Cheng Y, Xi C, Dai S, Ji C, Collu M, Li M, et al. Wave energy extraction and hydroelastic response reduction of modular floating breakwaters as array wave energy converters integrated into a very large floating structure. *Applied Energy*. 2022;306.
- [9] Koo W. Nonlinear time-domain analysis of motion-restrained pneumatic floating breakwater. *Ocean Engineering*. 2009;36:723-31.
- [10] Zhao X, Zhang L, Li M, Johanning L. Experimental investigation on the hydrodynamic performance of a multi-chamber OWC-breakwater. *Renewable and Sustainable Energy Reviews*. 2021;150.
- [11] Malara G, Arena F. Response of U-Oscillating Water Column arrays: semi-analytical approach and numerical results. *Renewable Energy*. 2019;138:1152-65.
- [12] Xu C, Liu Z, Tang G. Experimental study of the hydrodynamic performance of a U-oscillating water column wave energy converter. *Ocean Engineering*. 2022;265.
- [13] Moretti G, Malara G, Scialò A, Daniele L, Romolo A, Vertechy R, et al. Modelling and field testing of a breakwater-integrated U-OWC wave energy converter with dielectric elastomer generator. *Renewable Energy*. 2020;146:628-42.
- [14] Howe D, Nader J-R, Macfarlane G. Experimental investigation of multiple Oscillating Water Column Wave Energy Converters integrated in a floating breakwater: Energy extraction performance. *Applied Ocean Research*. 2020;97.
- [15] Howe D, Nader J-R, Macfarlane G. Experimental investigation of multiple oscillating water column

Hydroelastic performance of a flexible pontoon-type floating breakwater embedded with multiple oscillating-water-column devices

wave energy converters integrated in a floating breakwater: Wave attenuation and motion characteristics. *Applied Ocean Research*. 2020;99.

[16] Kim J-S, Nam BW, Park S, Kim K-H, Shin S-H, Hong K. Numerical investigation on hydrodynamic energy conversion performance of breakwater-integrated oscillating water column-wave energy converters. *Ocean Engineering*. 2022;253.

[17] Zhao X, Ning D, Zhang C, Liu Y, Kang H. Analytical Study on an Oscillating Buoy Wave Energy Converter Integrated into a Fixed Box-Type Breakwater. 2017;2017:3960401.

[18] Reabroy R, Zheng X, Zhang L, Zang J, Yuan Z, Liu M, et al. Hydrodynamic response and power efficiency analysis of heaving wave energy converter integrated with breakwater. *Energy Conversion and Management*. 2019;195:1174-86.

[19] Cheng Y, Fu L, Dai S, Collu M, Ji C, Yuan Z, et al. Experimental and numerical investigation of WEC-type floating breakwaters: A single-pontoon oscillating buoy and a dual-pontoon oscillating water column. *Coastal Engineering*. 2022;177.

[20] Cheng Y, Du W, Dai S, Ji C, Collu M, Cocard M, et al. Hydrodynamic characteristics of a hybrid oscillating water column-oscillating buoy wave energy converter integrated into a π -type floating breakwater. *Renewable and Sustainable Energy Reviews*. 2022;161.

[21] Martins-Rivas H, Mei CCJofM. Wave power extraction from an oscillating water column at the tip of a breakwater. 2009;626:395-414.

[22] Elhanafi A, Macfarlane G, Fleming A, Leong Z. Experimental and numerical investigations on the hydrodynamic performance of a floating-moored oscillating water column wave energy converter. *Applied Energy*. 2017;205:369-90.

[23] Elhanafi A, Macfarlane G, Ning D. Hydrodynamic performance of single-chamber and dual-chamber offshore-stationary Oscillating Water Column devices using CFD. *Applied Energy*. 2018;228:82-96.

[24] Tsai C-P, Ko C-H, Chen Y-C. Investigation on Performance of a Modified Breakwater-Integrated OWC Wave Energy Converter. *Sustainability*. 2018;10.

[25] Zhou Y, Ning D, Shi W, Johanning L, Liang D. Hydrodynamic investigation on an OWC wave energy converter integrated into an offshore wind turbine monopile. *Coastal Engineering*. 2020;162.

[26] Zheng S, Antonini A, Zhang Y, Greaves D, Miles J, Iglesias GJJoFm. Wave power extraction from multiple oscillating water columns along a straight coast. 2019;878:445-80.

[27] Peng C, Ning D, Zhou F, Chen L. Hydrodynamic performance of a leeward inlet OWC (LI-OWC) device for long-wave attenuation and power generation. *Renewable Energy*. 2026;256.

[28] Cheng Y, Du W, Dai S, Yuan Z, Incecik A. Wave energy conversion by an array of oscillating water columns deployed along a long-flexible floating breakwater. *Renewable and Sustainable Energy Reviews*. 2024;192.

[29] Gato L, Falcao AdF, Justino PA. Optimization of power take-off equipment for an oscillating water column wave energy plant. 2005.

[30] Casas I, Lekube J. Electricity forecast adapted to ocean conditions: The Mutriku case study. *Applied Ocean Research*. 2024;149.

[31] Allsop W, Bruce T, Alderson J, Ferrante V, Russo V, Vicinanza D, et al. Large scale tests on a generalised oscillating water column wave energy converter. *Proceedings of the HYDRALAB IV Joint User Meeting, Lisbon, Portugal 2014*. p. 2-4.

[32] Whittaker T, Beattie W, Folley M, Boake C, Wright A, Osterried M, et al. The Limpet wave power project—The first years of operation. 2004.

Hydroelastic performance of a flexible pontoon-type floating breakwater embedded with multiple oscillating-water-column devices

- [33] Collins I, Hossain M, Dettmer W, Masters I. Flexible membrane structures for wave energy harvesting: A review of the developments, materials and computational modelling approaches. *Renewable and Sustainable Energy Reviews*. 2021;151.
- [34] Algie C, Ryan S, Fleming A. Predicted power performance of a submerged membrane pressure-differential wave energy converter. *International Journal of Marine Energy*. 2017;20:125-34.
- [35] Smith WR. Wave–structure interactions for the distensible tube wave energy converter. *Proceedings of the Royal Society A: Mathematical, Physical and Engineering Sciences*. 2016;472.
- [36] Babarit A, Singh J, Mélis C, Watez A, Jean P. A linear numerical model for analysing the hydroelastic response of a flexible electroactive wave energy converter. *Journal of Fluids and Structures*. 2017;74:356-84.
- [37] Ancellin M, Dong M, Jean P, Dias F. Far-Field Maximal Power Absorption of a Bulging Cylindrical Wave Energy Converter. *Energies*. 2020;13.
- [38] Greaves D, Hann M, Kurniawan A, Chaplin J, Farley F. The hydrodynamics of air-filled bags for wave energy conversion. *International Conference on Offshore Renewable Energy* 2016.
- [39] Michele S, Buriani F, Renzi E, van Rooij M, Jayawardhana B, Vakis AI. Wave Energy Extraction by Flexible Floaters. *Energies*. 2020;13.
- [40] Zheng S, Michele S, Liang H, Meylan MH, Greaves D. Wave power extraction from a floating elastic disk-shaped wave energy converter. *Journal of Fluid Mechanics*. 2022;948.
- [41] Zheng S, Meylan MH, Zhu G, Greaves D, Iglesias G. Hydroelastic interaction between water waves and an array of circular floating porous elastic plates. *Journal of Fluid Mechanics*. 2020;900.
- [42] Liu Z, Xu C, Kim K, Zhang X, Ning D. Hydrodynamic and energy-harvesting performance of an isolated oscillating water column device: An experimental study. *Coastal Engineering*. 2024;189.
- [43] Teng Z, Cheng Y, Dai S, Yuan Z, Incecik A. Wave energy harvesting of a floating membrane carpet tethered by array-arranged power take-off units. *Renewable Energy*. 2025;254.
- [44] Ning D, Fu L, Zhou Y, Mayon R, Zhang Y. Hydrodynamic performance of a land-based multi-chamber OWC wave energy capture system: An experimental study. *Coastal Engineering*. 2024;190.
- [45] Montiel F, Bennetts L, Squire V, Bonnefoy F, Ferrant P. *Journal of Fluid Mechanics*. Hydroelastic response of floating elastic discs to regular waves. Part 2. Modal analysis. 2013;723:629-52.